A Study of Mn^{2+} Doping in CdS Nanocrystals

Angshuman Nag,[†] Sameer Sapra,[†,⊥] C. Nagamani,[†] Ajay Sharma,[‡] N. Pradhan,[§] S. V. Bhat,[‡] and D. D. Sarma*[,†,§]

Solid State and Structural Chemistry Unit and Department of Physics, Indian Institute of Science, Bangalore 560 012, India, and Centre for Advanced Materials, Indian Association for the Cultivation of Science, Kolkata 700 032, India

Received January 29, 2007. Revised Manuscript Received April 6, 2007

We report here the synthesis of water soluble Mn^{2+}-doped CdS nanocrystals in which it has been possible for the first time to obtain a distinct Mn^{2+} *d*-related emission well-separated from the defect state emissions. By varying the reaction temperature systematically, we establish 55 °C as the optimum temperature to maximize the Mn^{2+} *d* emission, the existence of this optimum synthesis temperature being shown as the result of two opposing influences of the temperature. Most interestingly, present results establish that Mn^{2+} favors preferential doping of larger-sized particles even within the narrow size distribution achieved in the present synthesis, rendering the relatively smaller-sized nanocrystals depleted of Mn^{2+} for any given synthesis. One important aspect of the present approach is that the synthesized nanocrystals readily dissolve in water without any deleterious effect on the Mn^{2+} *d*-related emission intensity.

Introduction

Semiconductor nanocrystals (NCs) have received enormous attention because of their size-dependent electronic[1−4] and optical[5−7] properties, making them potential candidates for various technological applications such as light-emitting diodes,[8,9] lasers,[10,11] and biological labels.[12] Independently, doping of bulk semiconductors has also proven to be yet another effective approach to tuning properties of such materials,[13] where the excitation takes place in the host semiconducting material, whereas the deexcitation involves the dopant energy levels via an energy transfer between the host and the dopant site. Thus, it is natural to find enormous excitement, effort, and success in controlling various properties of semiconducting materials by combining these two independent routes to functionalizing semiconducting materials, namely by tailoring the size of semiconducting NCs to tune their band gap suitably and doping diverse ions to introduce atomlike sharp energy levels into a variety of semiconducting NCs.[14−24] This combined approach opens up the possibility of realizing specific advantages of NCs, e.g., quantum confinement,[1−4] high quantum efficiency,[25−27] and resistance to photooxidation,[27] with those of doped semiconductors. At the simple level, doping of different luminescence activators in a semiconducting nanocrystal can tune the photoluminescence and electroluminescence at energies even lower than the band gap of the bulk material,[28,29] whereas the quantum size effect can tune the excitation energy with the size of the NCs without having a significant change in the energy of the activator related emission.

* Corresponding author. E-mail: mlsdds@iacs.res.in. Also at Jawaharlal Nehru Centre for Advanced Scientific Research, Bangalore 560054, India.
† Solid State and Structural Chemistry Unit, Indian Institute of Science.
‡ Department of Physics, Indian Institute of Science.
§ Centre for Advanced Materials, Indian Association for the Cultivation of Science.
⊥ Present address: Physikalische Chemie, Bergstr. 66b TU Dresden, 01097 Dresden.

(1) Sapra, S.; Shanthi, N.; Sarma, D. D. *Phys. Rev. B* **2002**, *66*, 205202.
(2) Sapra, S.; Sarma, D. D. *Phys. Rev. B* **2004**, *69*, 125304.
(3) Viswanatha, R.; Sapra, S.; Satpati, B.; Satyam, P. V.; Dev, B. N.; Sarma, D. D. *J. Mater. Chem.* **2004**, *14*, 661.
(4) Viswanatha, R.; Sapra, S.; Saha- Dasgupta, T.; Sarma, D. D. *Phys. Rev. B* **2005**, *72*, 045333.
(5) Murray, C. B.; Norris. D. J.; Bawendi, M. G. *J. Am. Chem. Soc.* **1993**, *115*, 8706.
(6) Nanda, J.; Sapra, S.; Sarma, D. D.; Chandrasekharan, N.; Hodes, G. *Chem. Mater*. **2000**, *12*, 1018.
(7) Peng, Z. A.; Peng, X. *J. Am. Chem. Soc.* **2001**, *123*, 183.
(8) Alivisatos, A. P. *J. Phys. Chem.* **1996**, *100*, 13226.
(9) Murray, C. B.; Kagan, C. R.; Bawendi, M. G. *Annu. Rev. Mater. Sci.* **2000**, *30*, 545.
(10) Kilmov, V. I.; Mikhailovsky, A. A.; Xu, S.; Malko, A.; Hollingsworth, J. A.; Leatherdale, C. A.; Eisler, H. J.; Bawendy, M. G. *Science* **2000**, *290*, 314.
(11) Vasa, P.; Singh, B. P.; Ayyub, P. *J. Phys. Condens. Matter* **2005**, *17*, 189.
(12) Chan, W. C. W.; Nie, S. *Science* **1998**, *281*, 2016.
(13) Furdyna, J. K. *J. Appl. Phys.* **1988**, *64*, R29.
(14) Bhargava, R. N.; Gallagher, D.; Hong, X.; Nurmikko, A. *Phys. Rev. Lett.* **1994**, *72*, 416.
(15) Alivisatos, A. P. *Science* **1996**, *271*, 933.
(16) Behboudnia, M.; Sen, P. *Phys. Rev. B* **2001**, *63*, 035316.
(17) Norris, D. J.; Yao, N.; Charnock, F. T.; Kennedy, T. A. *Nano Lett.* **2001**, *1*, 3.
(18) Malik, M. Z.; O'Brien, P.; Revaprasadu, N. *J. Mater. Chem.* **2001**, *11*, 2382.
(19) Hanif, K. M.; Meulenberg, R. W.; Strouse, G. F. *J. Am. Chem. Soc.* **2002**, *124*, 11495.
(20) Sapra, S.; Sarma, D. D.; Sanvito, S.; Hil, N. A. *Nano Lett.* **2002**, *2*, 60.
(21) Schwartz, D. A.; Norberg, N. S.; Nguyen, Q. P.; Parker, J. M.; Gamelin, D. R. *J. Am. Chem. Soc.* **2003**, *125*, 13205.
(22) Erwin, S. C.; Zu, L.; Haftel, M. I.; Efros, A. L.; Kennedy, T. A.; Norris, D. J. *Nature* **2005**, *436*, 91.
(23) Yang, Y.; Chen, O.; Angerhofer, A.; Cao, C. *J. Am. Chem. Soc.* **2006**, *128*, 12428.
(24) Pradhan, N.; Peng, X. *J. Am. Chem. Soc.* **2007**, *129*, 3339.
(25) Hines, M. A.; Guyot-Sionnest, P. *J. Phys. Chem.* **1996**, *100*, 468.
(26) Peng, X.; Schlamp, M. C.; Kadavanich, A. V.; Alivisatos, A. P. *J. Am. Chem. Soc.* **1997**, *119*, 7019.
(27) Jang, E.; Jun, S.; Pu, L. *Chem. Commun.* **2003**, 2964.
(28) Friend, R. H.; Gymer, R. W.; Holmes, A. B.; Burroughes, J. H.; Marks, R. N.; Taliani, C.; Bradley, D. D. C.; Santos, D. A. D.; Brédas, J. L.; Lögdlund M.; Salaneck, W. R. *Nature* **1999**, *397*, 121.
(29) Yang, H.; Holloway, P. H. *J. Phys. Chem. B* **2003**, *107*, 9705.

10.1021/cm0702767 CCC: $37.00
Published on Web 06/01/2007

In one of the early investigations in this direction, Bhargava et al. reported Mn^{2+} doping in ZnS NCs exhibiting a high quantum efficiency of the Mn^{2+} emission and a shortening of the lifetime to a few nanoseconds of the Mn^{2+} emission as compared to that in the bulk doped crystals (1.8 ms).[14] Since then, Mn^{2+} has been the most extensively studied luminescence activator in II−VI semiconductor NCs.[15−19] Subsequent studies[30−32] on Mn^{2+} doped ZnS and CdS NCs clarified that the lifetime of Mn^{2+} d−d transition does not change with quantum confinement, and the nanosecond decay time observed by Bhargava et al.[14] was interpreted as arising from broad defect state emissions from ZnS NCs. Unlike the case of Mn^{2+}-doped ZnS NCs with its well-resolved and easily identifiable Mn^{2+} related emission, the case of Mn^{2+}-doped CdS NCs has often been less clear.

Although Mn^{2+}-doped bulk CdS is usually prepared by thermal diffusion at a high-temperature (∼ 800 °C), corresponding NCs are prepared at a much lower temperature and doping Mn^{2+} in Cd^{2+} sites of CdS NCs is a challenging task. Many of the reported Mn^{2+}-doped CdS NCs synthesized so far have problems like poor Mn^{2+} emission, which is invisible at room temperature and appears only at low temperatures.[33] Moreover, defect state emissions and Mn^{2+} emission in Mn^{2+}-doped CdS NCs appear over the same energy region, giving a very broad emission without any distinctive feature in most of the reported PL spectra,[33−35] making it virtually impossible to distinguish the two contributions. Substantial efforts have been made to increase the quantum efficiency of the Mn^{2+} emission by modifying the surface[36] of the NCs and also forming[37] a CdS:Mn/ZnS core−shell NCs. It has also been known for some time that only a small fraction of the initial manganese concentration in the reaction mixture is actually incorporated in the lattice of the NCs with the excess manganese remaining outside, leading to a wrong estimation of manganese.[38] This is similar to the case of Mn^{2+}-doped ZnO, in which only a small amount of Mn^{2+} could be doped into the lattice.[39] Here, we report the doping of Mn^{2+} ions into CdS NCs at different reaction temperatures, establishing a narrow range of optimal temperature for the synthesis of this system with desirable PL properties. Our results suggest that the existence of an optimal synthesis temperature is the result of two opposing trends; although the incorporation of Mn^{2+} into the NCs is relatively more facile at lower temperatures, the quality of the generated NCs in terms of size dispesity, crystallinity, and the consequent presence of defect states within the band gap region improves with increasing synthesis temperature. Our investigations also firmly establish that at any given synthesis condition, Mn^{2+} is found to be incorporated preferentially in the relatively larger-sized NCs. To the best of our knowledge, the samples synthesized here provide the first example of well-separated Mn^{2+} emission from defect state emissions observed at room temperature, without requiring any surface modification in terms of a core−shell structure.

Experimental Section

$Cd(CH_3COO)_2{\cdot}2H_2O$, $Mn(CH_3COO)_2{\cdot}4H_2O$ and solvent dimethyl sulfoxide (DMSO) were purchased from Ranbaxy. $Na_2S{\cdot}9H_2O$ was obtained from Aldrich and the capping agent 1-thioglycerol from Fluka. The chemicals were used as received without further purification. A typical synthesis involved dissolution of Cd^{2+} (4-*y* mmol) and Mn^{2+} (*y* mmol) salts in 40 mL of DMSO; 0.5 mL of 1-thioglycerol was added to this solution, where the quantity *y* is four times the nominal Mn^{2+} percentage, *x*, in $Cd_{1-x}Mn_xS$. The reaction mixture was heated to the desired temperature in the 45−130 °C range with constant stirring, and a freshly prepared solution of S^{2-} in 10 mL of deionized water was added drop by drop to the DMSO solution over a period of ∼5 min. The reaction mixture was maintained at that fixed temperature for 12 h under an argon flow with continuous refluxing. A nonsolvent, acetone, was added in excess to the reaction mixture to precipitate out the nanocrystals, which was then centrifuged and washed thoroughly with methanol three times, followed by a washing with acetone to get rid of any Mn^{2+} and other unreacted ions remaining outside the clusters. A blank reaction was carried out only with Mn^{2+} and S^{2-} precursor, without adding Cd^{2+} precursor; this resulted in the formation of MnS with the space group $P6_{3mc}$ without showing any trace amount of other kinds of Mn compounds (see the Supporting Information). Mn^{2+}-doped bulk CdS was synthesized for use as a reference sample for EPR studies. Like the synthesis of NCs mentioned above, we carried out the reaction at 55 °C but without adding any capping agent; the powder obtained was sealed in a quartz tube at a high vacuum and heated at 700 °C for 30 h to obtain the bulk sample.

For size-selective precipitation, the nonsolvent acetone was added in two steps. In the first step, 45 mL of acetone was added, which helps to precipitate the larger particles; the reaction mixture was then centrifuged to collect the NCs followed by washing with methanol and acetone as before. Ten milliliters of extra acetone was added to the supernatant solution, which precipitated out the smaller particles, followed by centrifuging and washing as before.

Powder X-ray diffraction (XRD) patterns were recorded on a Siemens D5005 diffractometer using Cu Kα radiation. The diffracted intensities from these nanocrystals are generally weak and all patterns were recorded at a slow scan rate (10 s per 0.1°) to get a good signal-to-noise ratio. UV−visible absorption experiments were performed on a Perkin-Elmer's Lambda 35 UV−visible spectrometer, and Perkin-Elmer's LS 55 Luminescent spectrometer was used for photoluminescence measurements. All the UV−visible absorption spectra and PL spectra were recorded by redispersing the NC powder in DMSO except one aqueous dispersion, as mentioned in the next section. Atomic absorption spectroscopy (AAS) is an excellent tool for quantitative identification of trace amounts of a metal element in the presence of much higher concentrations of other elements, and the concentration of manganese with respect to that of cadmium was measured using Perkin-Elmer's AAnalyst 200, atomic absorption spectrometer, equipped with Perkin-Elmer lamps for Cd and Mn at wavelengths 228.8 and 279.5

(30) Sapra, S.; Prakash, A.; Ghangrekar, A.; Periasamy, N.; Sarma, D. D. *J. Phys. Chem. B* **2005**, *109*, 1663.
(31) Chamarro, M. A.; Voliotis, V.; Grousson, R.; Lavallard, P.; Gacoin, T.; Counio, G.; Boilot, J. P.; Cases, R. *J. Cryst. Growth* **1996**, *159*, 853.
(32) Bol, A. A.; Meijerink, A. *Phys. Rev. B* **1998**, *58*, R15997.
(33) Levy, L.; Feltin, N.; Ingert, D.; Pileni, M. P. *J. Phys. Chem. B* **1997**, *101*, 9153.
(34) Levy, L.; Feltin, N.; Ingert, D.; Pileni, M. P. *Langmuir* **1999**, *15*, 3386.
(35) Levy, L.; Ingert, D.; Feltin, N.; Pileni, M. P. *Adv. Mater.* **1998**, *10*, 53.
(36) Kim, D.; Miyamoto, M.; Takahashi, M.; Ikeuchi, K.; Nakayama, M. *Phys. Status Solidi C* **2004**, *1*, 835.
(37) Yang, H.; Holloway, P. H. *Appl. Phys. Lett.* **2003**, *82*, 1965.
(38) Cunio, G.; Gacoin, T.; Boilot, J. P. *J. Phys. Chem. B* **1998**, *102*, 5257.
(39) Viswanatha, R.; Sapra, S.; Sen Gupta, S.; Satpati, B.; Satyam, P. V.; Dev, B. N.; Sarma, D. D. *J. Phys. Chem. B* **2004**, *108*, 6303.

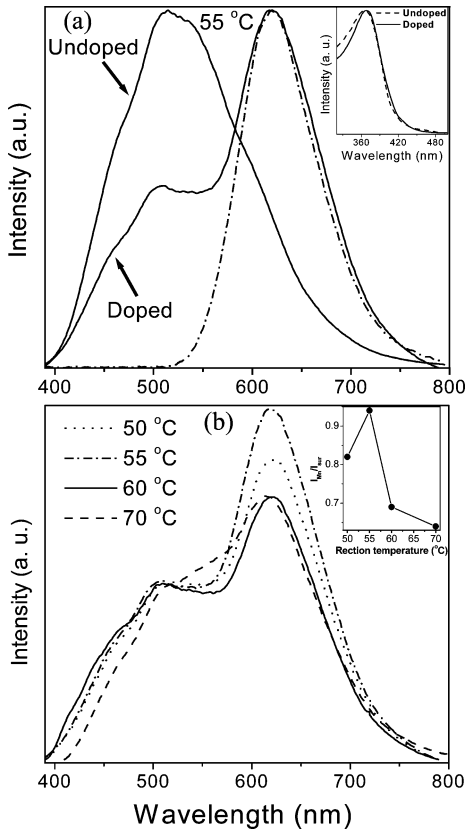

Figure 1. (a) PL spectra of the undoped and 1.9% Mn^{2+}-doped CdS NCs synthesized at 55 °C. The dash-dot line represents the PL spectrum of 1.9% Mn^{2+}-doped CdS NCs with a time delay of 50 μs. Inset shows the PLE spectra of the undoped and doped NCs corresponding to 514 and 620 nm emission, respectively. (b) PL spectra of the Mn^{2+}-doped CdS NCs synthesized at different temperatures with fixed Mn^{2+} precursor (25%) concentration. Inset shows the intensity ratio of Mn^{2+} *d* emission (I_{Mn}) to surface-state emissions obtained (I_{sur}) as a function of reaction temperature.

nm, respectively. Approximately 3.2 mg of the nanocrystal powder was dissolved in about 10 mL of 1:1 hydrochloric acid, diluted to 25 mL and used to estimate manganese concentration. A part of the solution used for estimating manganese concentration was diluted 100 times to estimate cadmium concentration, because manganese and cadmium have linear working ranges with upper limits approximately at 2.5 and 1.5 mg/L, respectively. A Tecnai F30 microscope at an accelerating voltage of 300 KeV was used for transmission electron microscopy (TEM). Electron paramagnetic resonance (EPR) measurements were carried out on powder samples at 9.5 GHz using a Bruker X-band spectrometer at room temperature.

Results and Discussion

The photoluminescence (PL) spectra of the undoped and 1.9% Mn^{2+}-doped CdS NCs synthesized at 55 °C are shown in Figure 1a; the absorption edge of both samples appears at ~373 nm. The PL spectrum of the undoped sample is broad with a peak at 514 nm, red-shifted from the band edge, characteristic of surface state emissions. Interestingly, the PL spectrum of the Mn^{2+}-doped nanocrystals shows a distinct, sharp feature at ~620 nm in addition to surface state emissions; evidently, this sharp emission feature with an intensity larger than that from the surface state is absent for the undoped NCs. This observation already suggests that the sharp emission feature at about 620 nm is indeed due to Mn^{2+} ions. We have collected the emission spectra with different delay times after the initial excitations in order to further probe the nature and origin of emission features; the result for a 50 μs delay is shown in Figure 1a. More delay spectra can be found in Figure 2 of the Supporting Information. These results make it clear that the lifetime associated with the surface state emissions is substantially less than 50 μs, being entirely absent in the spectra with a 50 μs delay. In contrast, we find that the emission peak at 620 nm associated with the Mn^{2+} d−d transition has a long lifetime that is visible even after 3 ms. These results also allows us to probe the Mn^{2+} d emission line shape without an overlapping contribution from surface states, while supporting the earlier reports[31,32] that the lifetime of Mn^{2+} d−d transitions does not reduce to the nanosecond scale with quantum confinement. The observed 620 nm peak for Mn^{2+} emission is red-shifted compared to the peak position for Mn^{2+} d-emission that has been earlier reported[23] at ~585 nm. However, very recently, Pradhan et al. reported[24] the tuning of Mn^{2+} emission peak from 582 to 610 nm in the same tetrahedral ZnSe nanocrystalline sample by exchanging the aliphatic amine capping agent with a thiolate ligand and suggested that because thiolate is a stronger ligand to II−VI semiconductor NCs, Mn^{2+} centers will experience less electric field difference along different directions. This results in a smaller splitting of the energy levels. It is possible that there is also an analogous decrease in the electric field at the Mn^{2+} site in these NCs as well, which might have caused the red-shift in Mn^{2+} emission. Photoluminescence excitation (PLE) spectra corresponding to 514 and 620 nm emissions for the undoped and doped samples, respectively, are shown in the inset to Figure 1a; we have also shown an expanded version of this figure in the Supporting Information for better clarity. These spectra exhibit maxima at ~370 nm corresponding to the band gap excitation of those CdS nanocrystal host. This clearly suggests that Mn^{2+} emission at 620 nm arises from Mn^{2+} ions being incorporated in to the CdS NCs. Energy transfer either directly from the conduction/valence bands and/or from the defect states excites Mn^{2+} ions that provide good traps for the excited electrons and holes, which then de-excite and emit at ~620 nm via the $^4T_1-^6A_1$ transition of Mn^{2+} d-states.[30] It is important to note here that earlier efforts to dope Mn^{2+} into CdS nanocrystals and therefore obtain the characteristic Mn^{2+} d-electron transitions have been largely impeded by the presence of a strong and overlapping PL feature arising from defect states of CdS, leading to a broad emission encompassing both the Mn^{2+} d−d transitions and defect state transitions in contrast to present result of a distinct Mn^{2+} d emission, well-separated from the surface state emissions of the host nanocrystals. One important difference between earlier approaches and present one appears to be that surface state emissions with peak at ~508 nm exhibited by these NCs are much more blue-shifted compared to earlier reports; this in turn allows us to observe a distinct PL signature for the Mn^{2+} d-emission (peak at ~620 nm) that is well-separated from surface state emissions (see the Supporting Information).

To optimize the synthesis conditions, we carried out the doping of Mn^{2+} into CdS NCs at various temperatures. A selected set of PL emissions from Mn^{2+}-doped CdS NCs

prepared at different temperatures are shown in Figure 1b, where we have normalized the surface-state emission intensity at 513 nm for an easy comparison. This plot makes it evident that there is a systematic variation in the emission intensity ratio between Mn^{2+} d emission and surface-state emissions with the reaction temperature. To quantify the variation in the ratio of the two intensities, namely the intensities associated with Mn^{2+} d emission (I_{Mn}) and with surface-state emissions (I_{sur}) to each of the PL spectrum shown in Figure 1b, we decomposed individual spectra in terms of surface and Mn^{2+} contributions. This was achieved by a least-square-error analysis of the experimental spectra using the PL spectrum of the undoped sample and time-delayed (50 μs) PL spectrum of the corresponding doped sample as references for surface and Mn^{2+} emission contributions, respectively. We have plotted this intensity ratio as a function of synthesis temperature in inset to Figure 1b, establishing 55 °C as the optimal reaction temperature to obtain the highest relative Mn^{2+} d emission. We have also shown absorbance-normalized PL data in Figure 4 of the Supporting Information, which clearly establishes that the Mn^{2+} d emission intensity is indeed maximized even in absolute terms for the NCs synthesized at 55 °C. The quantum efficiency of these NCs were found to be ~2%. All further results reported here are on this optimally synthesized sample, although we have obtained similar results for samples synthesized at other temperatures too.

In an attempt to dope different amounts of Mn^{2+} in CdS NCs, we carried out the synthesis with different starting concentrations of Mn^{2+} precursors. We have used AAS to find out the exact amount of Mn^{2+} present in the final reaction product containing nanocrystal powder. For 10, 20, 25, and 30% Mn^{2+} precursor used during the synthesis, we observe 0.9, 1.6, 1.9, and 1.8% Mn^{2+}, respectively, in the final product. These results confirm that, in spite of a high solubility (up to 45%) of Mn^{2+} in bulk CdS lattice[13] and our repeated efforts to dope higher concentrations of Mn^{2+}, the extent of doping is much less in these CdS NCs. The doping level increases gradually by increasing the Mn^{2+} precursor concentration from 10 to 25%, but a further increase in the Mn^{2+} precursor concentration up to 30% does not increase the doping level. We have estimated the Mn^{2+} concentration in the supernatant solution obtained after the precipitation and centrifugation of the product NCs and found that almost the entire amount of the Mn^{2+} remains in that solution. For example, during the synthesis of 1.9% Mn^{2+}-doped CdS NCs, 245 mg of a Mn^{2+} precursor that contains 54.94 mg of Mn^{2+} was used and the AAS results show that the 53.6 mg of Mn^{2+} remains in the solution after the NCs are precipitated out. This shows a poor reactivity of the Mn^{2+} precursor under the reaction condition, consistent with poor doping of the NCs.

We show the corresponding powder XRD patterns of these samples in Figure 2a. CdS NCs may crystallize in both wurtzite (WZ) and zinc blende (ZB) structures,[40,41] making

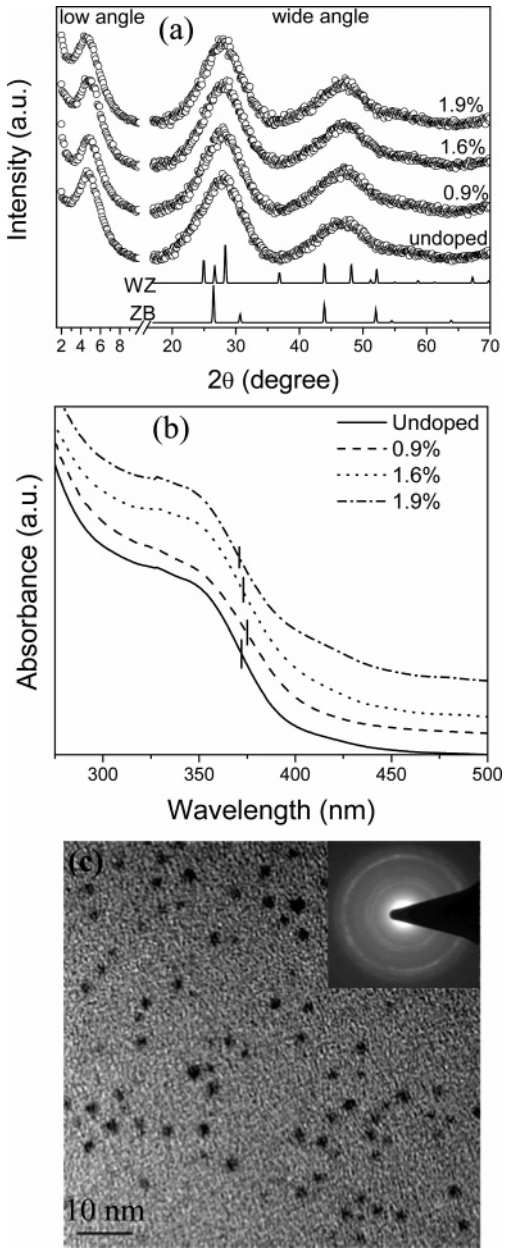

Figure 2. (a) Low-angle and wide-angle X-ray diffraction patterns for the undoped and Mn^{2+}-doped CdS NCs; bulk wurtzite (WZ) and zinc blende (ZB) patterns of CdS are also shown. (b) UV−visible absorption spectra of the undoped and Mn^{2+}-doped CdS NCs synthesized at 55 °C; the small vertical line in each spectrum indicates the point of inflection. (c) Transmission electron micrograph of 1.9% Mn^{2+}-doped CdS NCs.

it difficult to obtain unambiguous crystal structure information from the XRD patterns of these NCs because of large broadening and overlapping of cubic and wurtzite XRD patterns. However, it is more important to note that the undoped and all doped samples have almost identical XRD patterns with an equal extent of peak broadening, suggesting these NCs have similar size and crystal structure independent of Mn^{2+}-doping. The low-angle X-ray diffraction pattern shown in Figure 2a exhibits a peak at $2\theta \approx 4.6°$ for all samples independent of its Mn^{2+} content. This diffraction peak, in conjunction with Bragg's law, provides an estimate of the average interparticle separation,[42] which equals the diameter of the NCs, including the capping layer; the low-

(40) Banerjee, R.; Jayakrishnan, R.; Ayyub, P. *J. Phys. Condens. Matter* **2000**, *12*, 10647.
(41) Nanda, J.; Kuruvilla, B. A.; Sarma, D. D. *Phys. Rev. B* **1999**, *59*, 7473.
(42) Sapra, S.; Sarma, D. D. *Pramana* **2005**, *65*, 565.

angle peak in Figure 2a corresponds to 1.9 nm for all the samples synthesized at 55 °C, suggesting that the present synthesis approach allows us to dope Mn^{2+} into CdS NCs without causing any perceptible variation in the nanocrystal size.

Figure 2b shows the UV−visible absorption spectra of the Mn^{2+} doped and undoped CdS NCs. These spectra appear very similar to each other with the point of inflection determined from the dip in the derivative and marked with a short vertical line for each case in the figure, appearing at 373 ± 2 nm. This corresponds to a band gap of 3.32 ± 0.02 eV. The variation in the band gap of ± 0.02 eV for various samples is well within the experimental uncertainties, thereby suggesting very similar size for all those NCs independent of Mn^{2+} content. The increase in the band gap of the NCs compared to the bulk CdS band gap[43] of 2.42 eV (513 nm) is due to the quantum confinement effect in the nanometric size regime. Using the reported results of the band gap variation with size,[2] the size of these NCs was calculated to be 1.9 nm. Figure 2c shows the transmission electron micrograph of the 1.9% Mn^{2+}-doped CdS NCs confirming the size to be 2.1 nm with a size distribution of 12%. The average size obtained from the TEM data is in agreement with the size estimated from UV−visible absorption (1.9 nm) and low-angle XRD (1.9 nm). As mentioned earlier, low-angle XRD gives the diameter of the NCs including the capping layer; therefore, it is surprising to find the size estimate from this low-angle XRD measurment agreeing with the size estimated by UV−visible absorption, which does not account for the capping layer thickness. However, Nanda et al.[41] reported an effective capping layer thickness of ~2 Å for 2.5 nm CdS NCs using the same capping agent 1-thioglycerol as we used. Assuming a similar capping layer thickness in these NCs, the small underestimation of size by law angle XRD is possibly due to experimental uncertainties.

We now turn to certain intriguing aspects of emission and absorption properties of these doped NCs. Figure 3 shows a series of absorption, PL, and photoluminescence excitation (PLE) spectra of the same sized NCs synthesized at 55 °C with different Mn^{2+} doping concentrations. The left panels, a−c, show the absorption spectra in each case along with the PL spectra for two different excitation wavelengths; the specific excitation wavelengths are shown by the vertical arrows in relation to the absorption spectra in the same panel. The right panels, d−f, show the PLE spectra for the two emission wavelengths, 620 nm corresponding to Mn^{2+} d-related emission and 508 nm corresponding to surface-state emissions in each case. The PL spectra were also collected with a time delay of 50 μs to identify the Mn^{2+} d-related emission separated from surface-state emissions at shorter wavelengths; these spectra are shown in panels a−c with dashed−dotted lines. As expected, the relative intensity of the Mn^{2+} d-related emission in comparison to surface-defect-related emissions increases with an increasing dopant concentration. We note that an increase in the excitation wavelength to 480 nm, i.e., with an excitation energy (2.58 eV) substantially lower than the average absorption edge of ~373 nm (3.32 eV), does not give rise to any Mn^{2+} d-related emission, as shown in the Supporting Information. This confirms that the Mn^{2+} d-related emission involves energy transfer from the CdS host. More significantly, the relative intensities of different features in the PL spectra of the NCs change significantly when the excitation wavelength is changed from 370 to 400 nm, with the spectra in Figures 3a−c exhibiting a drastic increase in the Mn^{2+} d-related feature with 400 nm excitation in each case. Because there is invariably a finite, though narrow, size distribution of the synthesized NCs, there is obviously a corresponding distribution of bandgaps contributing to the spread of the absorption edge experimentally observed.[44] It is then logical to assume that a lower excitation energy of 3.10 eV (400 nm) in comparison to 3.35 eV (370 nm) would preferentially excite the larger-sized particles in the given distribution and unable to excite the smaller-sized ones. Thus, the observation of a higher Mn^{2+} d-related PL emission intensity when excited with 400 nm suggests that Mn^{2+} is not homogenously or statistically doped across the entire size distribution, but is

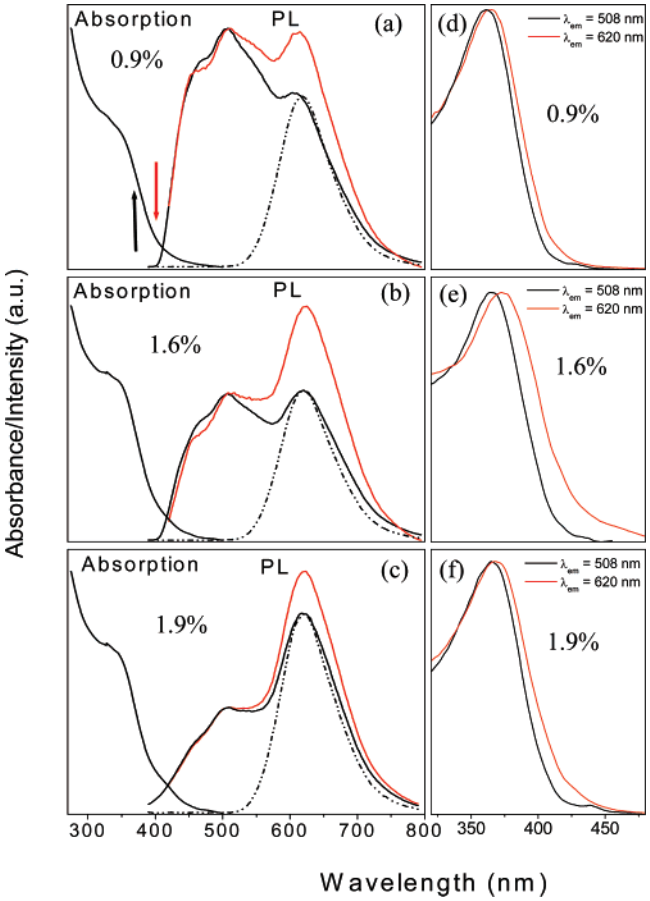

Figure 3. PL spectra of the Mn^{2+}-doped CdS NCs synthesized at 55 °C with different Mn^{2+} concentrations (a−c) excited at 370 (black line) and 400 nm (red line); the excitation wavelengths are indicated by black (370 nm) and red (400 nm) arrows on the corresponding UV−visible spectrum to point out the average size of the excited NCs at both excitation wavelength. All PL spectra in this figure are normalized at the highest intensity surface state emission, as evident from the figure. The black dash-dot line is the PL spectra excited at 370 nm with a time delay of 50 μs. PLE spectra (d−f) corresponds to 508 (black line) and 620 nm (red dashed line) emission.

(43) Kittel, C. *Introduction to Solid State Physics*, 7th ed.; John Wiley & Sons: New York; Chapter 8.

(44) Viswanatha, R.; Sarma, D. D. *Chem.—Eur. J.* **2006**, *12*, 180.

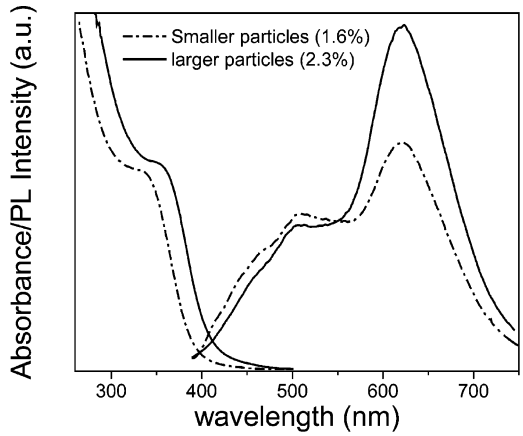

Figure 4. UV−visible absorption and PL spectra normalized by the corresponding integrated absorption spectra of the samples obtained after size-selective precipitation of 1.9% Mn^{2+}-doped CdS NCs synthesized at 55 °C. Absorption spectra were integrated down to the wavelength corresponding to the absorption maximum in each case. The PL spectra were excited with 375 nm radiation.

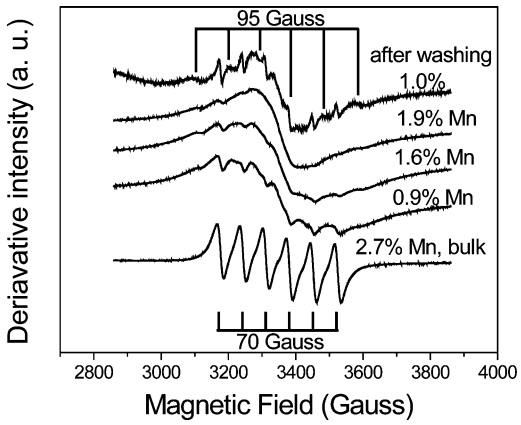

Figure 5. EPR spectra taken at 9.5 GHz and room temperature for powdered samples of Mn^{2+}-doped CdS NCs with different Mn^{2+} concentrations, bulk Mn^{2+}-doped CdS, and after washing the as prepared 1.9% Mn^{2+}-doped CdS NCs with dilute HCl. After being washed, the Mn^{2+} content is reduced to 1.0%. Two sets of vertical lines at the top and bottom of the figure indicate the sextet lines hyperfine splitting of 95 and 70 G, respectively.

preferentially doped into the larger sized NCs, making the smaller-sized ones less doped. This interpretation is also supported by the PLE spectra in the right panels of Figure 3. Those figures show that the PLE corresponding to the Mn^{2+} d−d transitions is a little red-shifted compared to that of surface-state emissions for each of the samples. Because surface-state emissions are contributed to by all sized NCs, red-shifted PLE spectra corresponding to Mn^{2+} d-related emission suggest that Mn^{2+} is preferentially present in the larger-sized NCs.

To establish this preferential doping of Mn^{2+} into the larger-sized NCs on a firm footing, we carried out a size-selective precipitation of the 1.9% Mn^{2+}-doped NCs synthesized at 55 °C. After collecting the presumably larger particles that precipitated out on addition of 45 mL of acetone, the smaller nanoparticles were collected from the supernatant solution obtained after isolating the larger particles by the addition of 10 mL of extra acetone. In Figure 4, we show comparative UV−visible absorption and PL spectra normalized by the corresponding absorption spectra of these two samples generated from a single synthesis of Mn^{2+}-doped CdS via postsynthesis size-selective precipitation. The particles collected by the first precipitation from the reaction mixture exhibit the band gap at 385 nm (3.22 eV) compared to 365 nm (3.40 eV) for the particles obtained from the supernatant solution, as shown by the absorption spectra in Figure 4. This suggests a larger size for the precipitated particles compared to the ones from the supernatant, establishing the efficacy of the size-selective precipitation process. From the well-established relationship between the shift in the band gap and the size of NCs,[2] we estimate the larger particles to have an average diameter of 2.1 nm, whereas the smaller particles are estimated to have an average diameter of 1.8 nm. In fact, the different-sized particles can be easily identified colorimetrically; the powder of the larger particles has a pale yellow color and that of the smaller particles has an off-white color (see the Supporting Information). AAS shows that the larger particles have 2.3% Mn^{2+} and the smaller particles have 1.6% Mn^{2+}. The PL spectra in Figure 4 clearly show that the PL intensity of Mn^{2+} d−d transitions is much higher for the larger particles than the smaller particles, suggesting a preferential Mn^{2+}-doping in the larger NCs. These results confirm that for nanocrystals synthesized at a particular reaction temperature, Mn^{2+} ions are preferentially incorporated in the larger-sized particles within the given size distribution of the synthesized NCs.

The EPR spectra recorded at 9.5 GHz and room temperature for all the Mn^{2+} doped CdS nanocrystal samples synthesized at 55 °C show some weak, partially resolved peaks superimposed on a broad background signal, as illustrated in Figure 5 for a few specific cases. The EPR spectrum of 2.7% Mn^{2+}-doped bulk CdS, used here as a reference material, shows the typical[38] six-line structure with a hyperfine splitting of 70 G, corresponding to substitutional Mn^{2+} ions at the tetrahedral Cd^{2+} sites. The broad signal in all nanocrystal spectra originates from the dipole−dipole interactions between the Mn^{2+} impurities and its relative contribution increases with an increase in Mn^{2+} concentration. Weakly resolved narrow bands in the EPR spectra of NCs are found to arise from two sets of sextet lines. The major contribution comes from the set with a hyperfine splitting of 70 G corresponding to isolated manganese ions incorporated in the tetrahedral CdS lattice, whereas the minor phase with a hyperfine splitting of 95 G corresponds to isolated manganese ions with different bonding environments present near the surface of the NCs.[45,46] The 1.9% Mn^{2+}-doped CdS NCs were washed thoroughly with dilute HCl (pH 2.5); this removes[38] undoped Mn^{2+} species surrounding the nanocrystal surface. AAS shows 1.0% Mn^{2+} in the washed sample that was 1.9% before washing; this shows that about half of the Mn^{2+} concentration remains on the surface of the NCs. After sample is washed, the intensity of the broad EPR signal decreases significantly and the tetrahedral lines become visibly more prominent, as shown in the figure. Thus, it appears that the dipolar interaction broadened spectral feature is preferentially from the clustered

(45) Kennedy, T. A.; Glasser, E. R.; Klein, P. B.; Bhargava, R. N. *Phys. Rev. B* **1995**, *52*, R14356.
(46) Mikulec, F. V.; Kuno, M.; Bennati, M.; Hall, D. A.; Griffin, R. G.; Bawendi, M. G. *J. Am. Chem. Soc.* **2000**, *122*, 2532.

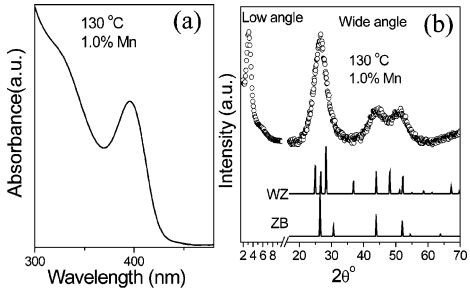

Figure 6. (a) UV−visible absorption spectrum of the 1.0% Mn^{2+}-doped CdS NCs synthesized at 130 °C. (b) Low-angle and wide-angle XRD patterns for the Mn^{2+}-doped CdS NCs synthesized at 130 °C and bulk WZ and ZB pattern of CdS.

Mn^{2+} surrounding the surface of the NCs, as it can be preferentially washed away with the help of a dilute acid. The acid wash, however, leaves the signals due to the two sets of sextets relatively unaffected, suggesting that these originate from deep within or from subsurface regions of NCs, accounting for the two different hyperfine splittings. We note that a 2 nm diameter CdS particle has on the order of 100 Cd^{2+} ions.[2] Therefore, a homogeneous doping of about 1% Mn^{2+}, as reported here, would require essentially each and every CdS nanocrystal to be doped with a single Mn^{2+} ion, if the doping would be perfectly uniform. This is obviously not the case, as suggested by the presence of the dipole broadened contribution in EPR spectra of every doped nanocrystal samples, representing clustering of several Mn^{2+} ions. Thus, it is inevitable that the remaining manganese ions, being insufficient to dope every nanocrystal, can dope only a certain fraction of the NCs and leave the rest undoped. A part of the doped NCs has isolated manganese ion in the CdS lattice exhibiting a hyperfine splitting of 70 G, whereas some others have isolated manganese ions near the subsurface region of the NCs showing a hyperfine splitting of 95 G. All the NCs doped with isolated Mn^{2+} ions are expected to contribute to the sharp PL emission near 620 nm (Figures 1 and 3), whereas the undoped NCs are the primary contributors for observed surface state emissions.

Noting that larger NCs tend to be preferentially doped at a given synthesis temperature, it appears natural to attempt achieving a higher level of Mn^{2+}-doping by deliberately synthesizing larger NCs, for example, by employing a higher reaction temperature. Thus, we synthesized CdS NCs at 130 °C in presence of 25% nominal manganese dopant ions much in the same way as the lower temperature synthesis, described in detail in the Experimental Section. The UV−visible absorption spectrum of this sample is shown in Figure 6a. From the absorption edge (411 nm), we obtain a band gap of 3.02 eV, corresponding to an average particle size of 2.6 nm.[2] Further, the absorption peak is considerably sharper compared to those shown in Figure 2b, suggesting a narrower distribution of particle size with the increase in the reaction temperature. The wide-angle XRD pattern (Figure 6b) with considerably narrower widths of the diffraction peaks compared to the those in Figure 2a for NCs synthesized at a lower temperature also suggest the formation of larger particles with the increase in the reaction temperature. The size of the nanocrystals estimated from the low-angle XRD (Figure 6b) using Bragg's low is 2.8 nm compared to 1.9 nm for those synthesized at 55 °C (Figure 2a). All these results establish the formation of larger-sized particles with the increase in the reaction temperature. In passing, we mention that we also synthesized undoped NCs at 130 °C; these particles exhibited essentially identical band gap and XRD pattern to the doped ones synthesized at 130 °C.

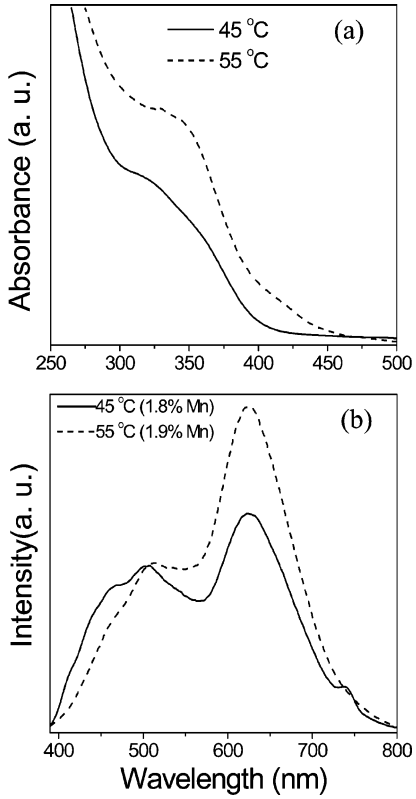

Figure 7. (a) UV−visible absorption spectra of the 1.8 and 1.9% Mn^{2+}-doped CdS NCs synthesized at 45 and 55 °C, respectively. (b) Comparison of the PL spectra of 1.8 and 1.9% Mn^{2+}-doped CdS NCs synthesized at 45 and 55 °C, respectively.

Interestingly, AAS showed only 1.0% of Mn^{2+} doped in these NCs synthesized at 130 °C, though we used 25% Mn^{2+} precursor concentration during the synthesis. This is a significantly lower level of doping compared to that (1.9%) achieved at 55 °C in spite of a larger average size of CdS NCs obtained at 130 °C. We recall here that a similar reaction carried out at 70 °C (Figure 1b) yielded a doping level of 1.4%. In fact, we find that increasing synthesis temperature leads to a systematic decrease in the actual level of Mn^{2+} doping in CdS. This observation is consistent with the earlier report of Levy et al.[33]suggesting an expulsion of manganese ions from the interior of Mn^{2+}-doped CdS NCs on annealing beyond 80 °C.

We also carried out reaction at a lower temperature, 45 °C, in an attempt to dope a larger amount of Mn^{2+}. Figure 7a shows a broad UV−visible absorption spectrum of Mn^{2+} doped CdS NCs synthesized at 45 °C, indicating a larger size distribution compared to the NCs synthesized at 55 °C. AAS shows that for nominal 25% Mn^{2+} doping in which the reaction temperature is kept at 45 °C, the amount of Mn^{2+} present in the nanocrystal product is 1.8%, which is very close to the 1.9% Mn^{2+} obtained by synthesizing the NCs at 55 °C. Though the percentage of Mn^{2+} in the NCs remains more or less the same whether synthesized at 45 or 55 °C,

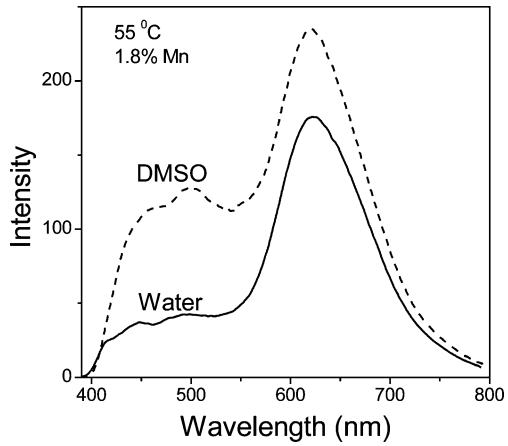

Figure 8. Comparison of the PL spectra of 1.8% Mn-doped CdS NCs synthesized at 55 °C dispersed in DMSO and deionized water.

the relative PL intensity of the Mn^{2+} d emission with respect to defect-state emissions of the NCs synthesized at 45 °C decreases significantly compared to that of the NCs synthesized at 55 °C, as shown in Figure 7b. The relative decrease in the Mn^{2+} d emission efficiency of the NCs synthesized at 45 °C may be attributed to the lower crystallinity of the NCs, enhancing the contribution from defect-state emissions.

NCs with a high PL efficiency, high resistance to photobleaching, broad excitation spectrum, and narrow emission spectrum are reported as suitable fluorescence sensors in biological applications.[47,48] However, NCs are mostly synthesized in nonpolar organic solvents and the key issue for any biological application is the water solubility of these nanocrystals.[48] Many efforts[49] have been made to solubilize NCs in aqueous buffers by replacing the hydrophobic layers on the surface of the NCs by amphiphilic ones. Unfortunately, in many such cases, there is a drastic decrease in the PL efficiency concomitant with the surface modification.[12,50] 1-Thioglycerol-capped Mn^{2+}-doped CdS NCs synthesized by us are soluble in water. Figure 8 compares the PL spectra of the 1.8% Mn^{2+}-doped NCs synthesized at 55 °C dispersed in deionized water with that of the NCs dispersed in DMSO. The efficiency of surface-state emissions decreases to a large extent in the aqueous dispersion of the NCs compared to that of the DMSO dispersion, but the efficiency of the Mn^{2+} d−d transitions of the aqueous dispersion is essentially unaffected. This, therefore, suggests that such samples can be used for biological labeling. In this context, another problem for biological applications is the autofluorescence of the biomolecules, which masks the signals from labeled molecules. Mn^{2+} d−d transitions with its fluorescence lifetime in milliseconds can be used to separate their signal from shorter-lifetime (nanosecond scale) fluorescence of biomolecules, enabling one to detect the labeled molecules.

Conclusions

Highly crystalline CdS and Mn^{2+}-doped CdS NCs with a narrow size distribution were synthesized with the average size ranging from 1.9 to 2.6 nm. With the help of AAS, it is shown that only a small percentage of Mn^{2+} ($\leq$2.3%) is associated with the nanocrystal samples in spite of the presence of a large (25%) Mn^{2+} concentration in the reaction mixture. It is shown that the PL spectra of the doped NCs exhibit Mn^{2+} d-electron transitions around 620 nm, clearly separated from surface-state emissions with a maximum near 508 nm; this is the first example of such a clear separation between the Mn^{2+}-dopant emission and surface-state emissions in Mn^{2+}-doped CdS nanocrystals. Exciting the samples with energies lower than the band gap energies of host nanocrystals but higher than the Mn^{2+} d−d transition energy does not give rise to any measurable Pl intensity, establishing that the Mn^{2+} d−d transition takes place following an energy transfer from CdS host NCs to the dopant site. The presence of surface-state emissions along with Mn^{2+} d emission for all samples suggests nonuniform doping of the NCs; this interpretation is further supported by EPR and other experiments. Systematic dependencies of the PL and PLE on the excitation and emission energies, respectively, indicate that the larger-sized NCs are preferentially doped by Mn^{2+} compared to the smaller-sized ones, even within the narrow size distribution achieved for a specific reaction condition. This surprising phenomenon is conclusively proven by carrying out a size-selective precipitation of a given sample of NCs into a group of large particles and a separate group of smaller particles and characterizing the size-separated groups for their Mn^{2+} content as well as their spectroscopic properties. The present investigation shows that 55 °C is the optimum reaction temperature to maximize the Mn^{2+} d emission intensity; at higher temperatures, Mn^{2+} is annealed out of the substitutional sites, leading to a lower level of doping, whereas a lower temperature of synthesis leads to less crystalline materials and consequent higher emission via defect states relative to Mn d emission. Finally, we also showed that these Mn^{2+}-doped CdS NCs are soluble in water without any perceptible effect on the Mn^{2+} d emission intensity, unlike many other systems, thereby suggesting possible biological applications.

Acknowledgment. The authors acknowledge the Department of Science and Technology and Board of Research in Nuclear Sciences, Government of India, for funding the project. D. D. Sarma acknowledges the National J. C. Bose Fellowship. Angshuman Nag acknowledges CSIR, Government of India, for a fellowship.

Supporting Information Available: XRD pattern of MnS, PL spectra with different delay times, PLE spectra of the undoped and 1.9% doped NCs, PL emission spectra normalized by the corresponding absorption spectra for different synthesis temperature, PL spectra with excitation energy less than band gap, photographs of the powders of larger and smaller particles obtained by size-selective precipitation and a discussion regarding a probable cause for well-separated Mn^{2+} emission from surface state emissions. This material is available free of charge via the Internet at http://pubs.acs.org.

CM0702767

(47) Larson, D. R.; Zipfel, W. R.; Williams, R. M.; Clark, S. W.; Bruchez, M. P.; Wise, F. W.; Webb, W. W. *Science* **2003**, *300*, 1434.
(48) Michalet, X.; Pinaud, F. F.; Bentolila, L. A.; Tsay, J. M.; Doose, S.; Li, J. J.; Sundaresan, G.; Wu, A. M.; Gambhir, S. S.; Weiss, S. *Science* **2005**, *307*, 538.
(49) Shavel, A.; Gaponik, N.; Eychmulller, A. *J. Phys. Chem. B* **2006**, *110*, 19280.
(50) Pathak, S.; Choi, S. K.; Arnheim, N.; Thompson, M. E. *J. Am. Chem. Soc.* **2001**, *123*, 4103.